Role of Steric Interactions on the Ionic Permeation Inside Charged Microgels: Theory and Simulations

Irene Adroher-Benítez, Silvia Ahualli, Alberto Martín-Molina, Manuel Quesada-Pérez, Arturo Moncho-Jordá*

Abstract

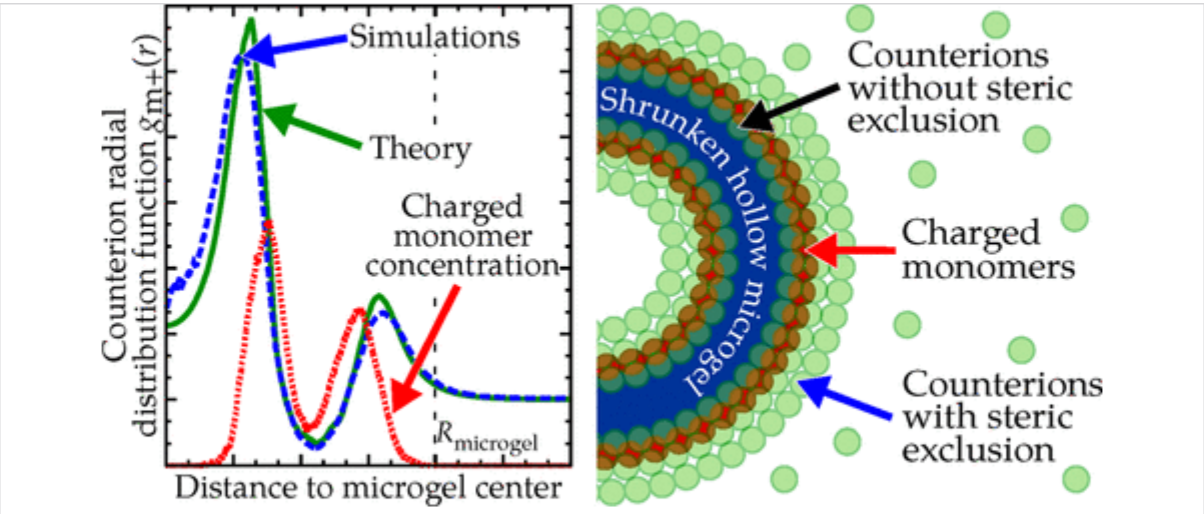

In this work, we study the effect of the steric excluded-volume interactions between counterions and thermoresponsive ionic heterogeneous microgel particles. With this aim, we perform Monte Carlo simulations to calculate the microgel effective net charge and the conunterion distribution function inside and around the microgel for different degrees of swelling. These results are compared to the ones obtained solving the Ornstein–Zernike integral equations within the HNC approximation. For this purpose, the equilibrium polymer mass and charge distribution inside the microgel resulting from simulations are used as the input for the integral equations. Two different models are considered to quantify the microgel-ion steric interaction. The model that considers polymer fibers formed by spheres demonstrates to be a very reliable way to predict counterion permeation in such microgels. Finally, integral equations are solved ignoring the steric interaction as well, in order to determine to what extent this effect is playing a significant role. The comparison between both predictions allows us to conclude that the microgel-ion steric repulsion has relevant effects on the counterion permeation if the polymer volume fraction of the microgel is high enough, and that the integral equation theory is a powerful tool to quantitatively predict the local density profiles of ions inside and around the microgel, even in situations where the internal microgel charge and mass density are nonhomogeneous.

Introduction

The term microgel refers to a “colloidal suspension of gel particles”. (1) That is, they are porous particles formed by cross-linked polymer chains dispersed in a solvent. They are also called nanogels, as their diameter usually varies from 10 to 1000 nm. Their main feature is the ability to swell or shrink as a response to a wide variety of parameters such as temperature, pH, solute concentration, or solvent nature. (2, 3) Microgels respond to external stimuli much faster than macroscopic gels, with a velocity increased by some orders of magnitude. (1) This feature is an advantage for a broad range of biotechnological applications. (4) In particular, the design of new intelligent drug transport and delivery systems is gaining attention in recent years. (5-7) Microgel particles are suitable for this purpose, since a therapeutic molecule can be encapsulated inside the particle and be transported to different parts of the human body, avoiding its degradation before it reaches the place where it has to be released. (8) With this aim, microgels and the interaction with different solutes, such as drugs and DNA, are being widely investigated. (9-12)

Ionic microgels, formed by cross-linked polyelectrolyte chains, are essential for most of biomedical applications, because drugs and other biomolecules are usually charged solutes dissolved in the medium where microgels are dispersed. For this reason, many authors have developed theoretical studies to analyze the permeation of ions and solutes inside microgels and to estimate the swelling equilibrium state of the particle. (13-16) Most of these works assume that ion permeation inside the microgel is controlled exclusively by the electrostatic interactions. In principle, this is a good approximation for loose, expanded microgel networks, where the pore size between polymer fibers is large enough to guarantee that ions can freely penetrate. However, this may not be the case of denser shrunken microgels, where the large packing fraction of the polymer network exerts an additional excluded volume repulsion that might partially hinder the migration of ions or other kind of solutes to the region inside the particle. This repulsive force is usually referred as steric interaction, and its study is the main goal of this work. Although there does not exist a general equation for the steric interaction between a cross-linked microgel and an incoming solute or ion valid for every type of particle, there are some approximated models that assume certain morphologies of the polymer network. These are based on the equilibrium partitioning effect, which states that solute concentration inside a neutral porous medium is smaller than the one in the bulk solution. (17)

In this work we focus on the effect that the microgel-ion steric repulsive interaction has on the permeation of counterions inside microgel particles that become heterogeneous as temperature increases. For this purpose, we use a novel hybrid method that blends Ornstein–Zernike integral equations and Monte Carlo simulations. On the one hand, Monte Carlo simulations have been previously used to study volume exclusion effects in gel systems with neutral solutes (18) so they are expected to be appropriate also for microgel particles. Even though this method requires more computational resources than integral equations, it provides accurate predictions of the equilibrium distribution of the cross-linked polymer network and the ionic density profiles. Microgel particles are simulated using a coarse-grained model, the so-called *bead–spring* model. This model has been widely used in Monte Carlo and molecular dynamics simulations of different polyelectrolytes, (19-26) gels, (27-30) microgels, (31-34) and even more complex mesoscopic systems (e.g., viruses (12)). Moreover, it has been successfully employed to compare simulation results with experimental swelling data of microgel particles, not only qualitatively but quantitatively as well. (35)

On the other hand, Ornstein–Zernike integral equations with HNC closure relations have demonstrated to be a powerful tool to study the permeation of ions inside microgel particles. (36) We solve these equations for the three-component system microgel-*co*ion-counterion using as input parameters the equilibrium density profiles of charged monomers and the polymer mass distribution obtained from simulations. This method allows the calculation of the radial distribution functions and, from them, the density profiles of ions inside and around the microgel particle. These results constitute a novelty in the sense that we are able to predict not only the net permeation of ions inside the microgel, but also to determine the region where they become preferentially adsorbed. (36, 37) The integral equations formalism is also especially useful because it takes explicitly ion–ion correlations into account. These correlations, which arise from the finite size of the ions, can be very important at high electrolyte concentration, in regions where they are strongly confined or close to colloidal surfaces. (38) Moreover, nonlinear effects resulting from highly charged colloid-ion systems can be studied with this method as well. The combination of simulations and integral equations provide a method to clearly estimate to what extent excluded volume forces influence the ionic permeation inside fibrous microgels.

Two important properties have been obtained using both methods, namely the microgel effective charge and the counterion and coion radial distribution functions. On the one hand, the effective charge is defined as the sum of the total charge of the porous particle, considering as well inner ions, with their respective positive or negative charge. This magnitude strongly depends on the number of counterions that have penetrated inside the microgel particle, and represents an estimate of how efficiently the microgel bare charge has been screened. Its importance may be seen in many aspects. For instance, effective charge controls the volume phase transition of charged microgel particles under weak screening conditions. (39) Moreover, stability of the suspensions strongly depends on this quantity, because it controls the electrostatic interaction between colloidal particles. (36, 40) On the other hand, the ionic density profiles provide detailed information about where ions are preferentially adsorbed inside the microgel particles, which is in general difficult to achieve experimentally. This is really helpful to study the local effects of microgel-ion interaction that arise for highly charged microgels and low ionic strengths. Up to now, most studies regarding interaction of solute with gels and microgels have been performed considering that the polymer packing fraction and the charge distribution inside the microgel are homogeneous. (41-43) However, when solute concentration is low and microgel charge distribution is nonhomogeneous, the counterion adsorption inside the microgel becomes highly dependent on the charge and polymer mass distribution. These local effects are expected to have a relevant effect on many microgel applications, in particular in drug transport and delivery.

In addition, by comparing the results given by both integral equations and Monte Carlo simulations we show that electrostatic interactions are not enough to describe the ionic permeation inside the microgel in thermal conditions at which the particle is collapsed. This finding supports the inclusion of an additional steric microgel-ion repulsion in the theoretical model to correctly explain ionic permeation close to the shrunken state. Once this steric effect is taken into account, the comparison between theory and simulations is in general very good.

This paper is organized in the following manner. In the first section we describe the theoretical framework and explain the numerical resolution of Ornstein–Zernike integral equations. Monte Carlo simulations are described in the next section. Then, the results obtained by both methods are shown and discussed, and finally, the conclusions of this work are summarized.

Theory

The system under study is a mixture of spherical microgel particles dispersed in water with 1:1 electrolyte. As the solvent is considered a background continuum, the system is formed by a ternary mixture in equilibrium of N_m microgels, N_+ counterions, and N_- coions. Their bare charges are given, respectively, by −Ze, $+e$, and $-e$, with e being the elementary charge. Hence, to fulfill electroneutrality we get $N_+ = N_- + ZN_m$. Polymer mass distribution and charge distribution inside the microgel network are obtained from the Monte Carlo simulation results.

Particle Interactions

In order to apply the integral equation method is necessary to define the pair interactions between any type of particle of the system (counterions, coions and microgel particles). Ion–ion interaction is assumed to be a combination of a short-range hard-core potential with a long-range Coulombic tail

$$\beta V_{ij}(r) = \begin{cases} \infty & r \leq (\sigma_i + \sigma_j)/2 \\ \dfrac{z_i z_j l_B}{r} & r > (\sigma_i + \sigma_j)/2 \end{cases} \quad (1)$$

where r is the distance between the centers of the ions, σ_i and z_i are, respectively, the diameter and valence of particle i, and $\beta \equiv 1/(k_B T)$. l_B is the so-called Bjerrum length, defined as $l_B \equiv e^2/4\pi \epsilon_r \epsilon_0 k_B T$, where ϵ_0 is the vacuum permittivity, k_B is the Boltzmann constant, and T the absolute temperature. The Bjerrum length also depends on temperature T through the relative permittivity ϵ_r. In this work, we assume that the solvent is water, with a permittivity given by the following T-dependence (44)

$$\epsilon_r(T) = 5321T^{-1} + 233.76 - 0.9297T + 0.1417 \times 10^{-2}T^2 - 0.8298 \times 10^{-6}T^3 \quad (2)$$

It is important to note that this pair interaction takes the finite size of the ions into account, which can induce relevant correlations at sufficiently large electrolyte concentration.

In order to obtain realistic predictions for ion penetration inside the microgel particle, a suitable model for microgel-ion interaction is required. When ions diffuse through microgel pores, electrostatic interaction may not be the only one that intervenes. There might be also an effective steric repulsion, whose relevance increases as microgel shrinks, that prevents the ion permeation. This repulsion is present even in the limit of point-like ions, since part of the volume available for the ion is already occupied by the polymer fibers. For ions of finite size, the excluded volume effect becomes logically more important, as ions also have to fit inside the internal pores of the microgel. Here, we assume that the microgel-ion potential can be split into two additive contributions, given by the electrostatic and steric terms, respectively

$$V_{mi}(r) = V_{mi}^{elec}(r) + V_{mi}^{ster}(r) \quad (3)$$

This potential only depends on the distance between the ion and the microgel center, r, because microgel particles are considered spherical. The electrostatic contribution can be calculated from the equilibrium spatial distribution of charged monomers. Note that in this work we do not assume any model for the distribution of charged groups inside the microgels, but instead, we use the distribution actually obtained from the Monte Carlo simulations. The expression of the electrostatic interaction potential between the microgel and certain ion located outside the microgel at a distance r from the its center can be expressed as

$$\beta V_{\mathrm{mi}}^{\mathrm{elec}}(r) = -\frac{Z z_i l_{\mathrm{B}}}{r}, \quad r > R_{\mathrm{m}} \tag{4}$$

where R_m is the external radius of the microgel. For $r < R_m$, the electrostatic interaction depends on the specific distribution of charged groups and must be obtained numerically from the electric field generated by the microgel particle, $E(r)$:

$$\beta V_{\mathrm{mi}}^{\mathrm{elec}}(r) = \beta V_{\mathrm{mi}}^{\mathrm{elec}}(R_{\mathrm{m}}) - z_i \int_r^{R_{\mathrm{m}}} E(r)\, \mathrm{d}r, \quad r \le R_{\mathrm{m}} \tag{5}$$

From Gauss's law, the electric field is given by

$$E(r) = -\frac{e Z_{\mathrm{in}}(r)}{4\pi \epsilon_r \epsilon_0 r^2} \tag{6}$$

where $Z_{in}(r)$ is the number of charged monomers enclosed within a sphere of radius r. It is calculated by integration of number density of charged monomers, $\rho_c(r)$, which is directly obtained from the simulations:

$$Z_{\mathrm{in}}(r) = \int_0^r 4\pi r'^2 \rho_c(r')\, \mathrm{d}r' \tag{7}$$

The next step involves the deduction of some expression for the steric repulsion that appears when an uncharged solute permeates through the polymeric microgel network and experiences the volume exclusion exerted by the polymer fibers. This interaction depends on the size of the incoming solute, the size of monomeric units, the polymer packing fraction and, in general, on the internal morphology of the microgel polymer network. In this work we use two different models previously employed by several authors. (17, 36, 45) In the first one the internal structure of the microgel is approximated by an assembly of randomly placed spherical monomers. (46) The second model (also called the Ogston model (47)) assumes that the internal polymer distribution is given by an assembly of infinitely long cylinders of constant radius, which are randomly distributed and mutually interpenetrable. Both of them may be expressed as the following equation for the steric microgel-ion interaction

$$V_{\mathrm{mi}}^{\mathrm{ster}}(r) = -\ln[1 - \phi(r)]\left(1 + \frac{\sigma_{\mathrm{i}}}{\sigma_{\mathrm{f}}}\right)^n \tag{8}$$

where $\phi(r)$ is the local polymer volume fraction inside the microgel, σ_i is the diameter of the incoming ion, and σ_f stands for the typical size of an elementary unit of the polymer network. The exponent n is given by $n = 3$, if we assume that the microgel is formed by an assembly of spherical monomers, and $n = 2$, if we use the Ogston model instead. In the first case, σ_f corresponds to the monomer diameter, σ_{mon}. In the second case, the effective diameter of the fiber is given by $\sigma_f = (2/3)^{1/2}\, \sigma_{mon}$. (18)

It should be emphasized that both analytical expressions for the steric repulsion have been corrected to take the overlapping volume between the polymer fibers into account. (48) As a result of this, both models are consistent with the limiting cases of high and low volume packing fraction. That is, for ϕ(*r*) → 0 there is enough room for ions to penetrate, so $V_{mi}^{ster} \to 0$. If the polymer volume fraction is very high, the microgel tends to behave as an impenetrable hard sphere, so $V_{mi}^{ster} \to \infty$.

In Figure 1, both microgel-ion steric potentials are plotted as a function of the polymer packing fraction, using the same parameter values considered in simulations and theoretical calculations. It is observed that the steric interaction is more repulsive for exponent $n = 3$ than for $n = 2$. For $\phi \to 1$, both interactions diverge, so the microgel becomes an impenetrable particle.

Figure 1

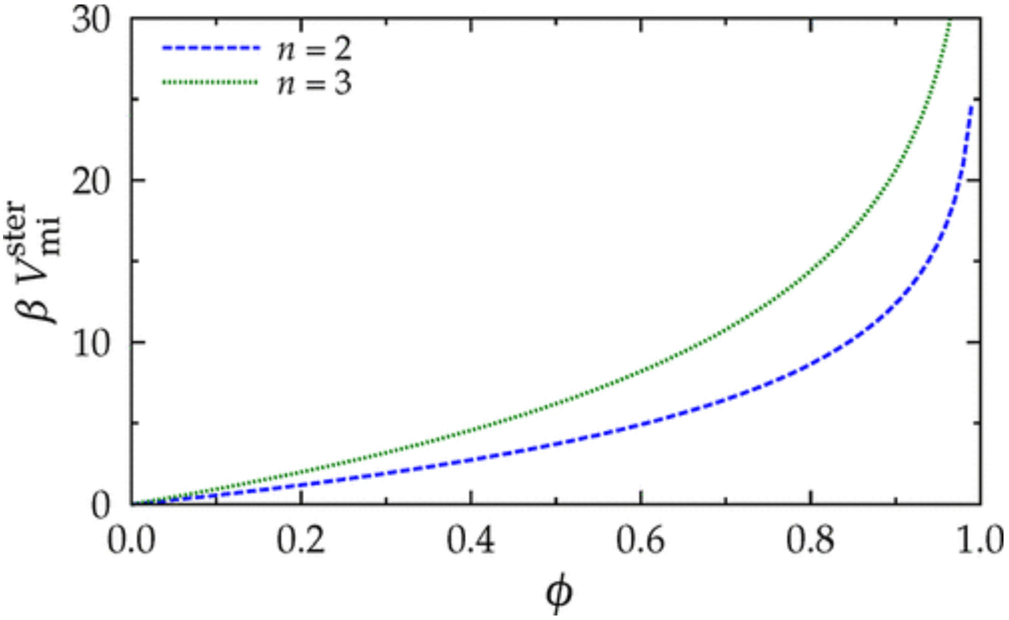

Figure 1. Microgel-ion steric potential as a function of microgel volume packing fraction. Blue dashed curve corresponds to $n = 2$ (Ogston model), while the green dotted to $n = 3$, in eq 8. To calculate $\beta V_{mi}^{ster}(r)$, we have used the same values considered in simulations and theoretical calculations, that is, $\sigma_{ion} = 0.7$ nm, $\sigma_{mon} = 0.65$ nm, and $\sigma_f = (2/3)^{1/2}\, \sigma_{mon}$.

Finally, the bare microgel–microgel interaction should also be known in order to obtain correct theoretical predictions for suspensions at finite microgel concentration. This interaction is in principle really difficult to determine, specially when microgels are in overlapping configurations, in which elastic forces arise in addition to the electrostatic ones. However, in this work we are only interested in the study of the ionic density profiles around a single microgel in the limit of infinite dilution of particles. Hence, there is no need to include this interaction in the theoretical background.

Ornstein–Zernike Integral Equations

The equilibrium radial distribution functions of counterions and coions around and inside the microgel particle, $g_{mi}(r)$, can be obtained by solving the Ornstein–Zernike (OZ) integral equations for the microgel (m), counterion (+) and coion (−) mixture. For a three-component mixture, the OZ equations are written in the Fourier space as a set of six algebraic equations,

$$\hat{h}_{\mu\nu}(k) = \hat{c}_{\mu\nu}(k) + \sum_{\lambda=1}^{3} \rho_{0\lambda}\hat{c}_{\mu\lambda}(k)\hat{h}_{\lambda\nu}(k) \quad (9)$$

where $\hat{h}_{\mu\nu}(k)$ and $\hat{c}_{\mu\nu}(r)$ are the Fourier transforms of the total and direct correlation functions, respectively, and $\rho_{0\lambda}$ stands for the number density of component λ in the bulk. In the limit of very dilute microgel suspension ($\rho_{0m} \to 0$) the six equations are decoupled into three groups which can be solved in three different steps. In the first step, the ion–ion correlations are calculated. Then, they are used in the second step to determine the microgel–counterion and microgel–coion correlations by solving the following set of two equations. Finally, there is still remaining a last integral equation which provides the microgel–microgel correlation. This last equation allows the calculation of the effective interaction between microgels particles induced by the presence of electrolyte. However, in this work we are not interested in this property, so we omit this part and focus on the microgel–ion correlations. As this procedure has been already used in previous works, (13, 36, 37) we encourage the reader to dip into them for further details.

In order to solve these equations, it is strictly necessary to complete them with additional closure relations connecting $\hat{h}_{\mu\nu}(r)$ and $\hat{c}_{\mu\nu}(r)$ with the interparticle interaction potentials $V_{\mu\nu}(r)$ (defined in eqs 1 and 3). In this work, the *Hypernetted-chain approximation* (HNC) (49) is used, due to the fact that it has demonstrated to be a quite precise approximation for the kind of interactions involved in mixtures of ionic microgel suspensions with electrolyte. (13, 36, 37) It is given by the following equation:

$$h_{\mu\nu}(r) = e^{h_{\mu\nu}(r)-c_{\mu\nu}(r)-\beta V_{\mu\nu}(r)} - 1 \quad (10)$$

To solve OZ-HNC equations, we make use of the Picard method of successive approximation. (50) Once calculated $h_{\mu\nu}(r)$ and $c_{\mu\nu}(r)$, radial distribution functions can be obtained straightforwardly

$$g_{\mu\nu}(r) = \frac{\rho_{\mu\nu}(r)}{\rho_{\nu 0}} = h_{\mu\nu}(r) + 1 \quad (11)$$

Picard method starts with an approximated initial guess for the direct correlation functions, $c_{\mu\nu(0)}$, and after an iteration, a new value $c_{\mu\nu(1)}$ is calculated. The procedure is repeated until convergence of the two last steps of the method is achieved.

However, for highly charged microgels, as the one object of this study, Picard method does not converge in just one realization. It is necessary to develop an adaptive method to increase gradually the microgel charge Z, which enhances the numerical convergence: the last value of $c_{\mu\nu}(i)$ calculated is used in the next realization of Picard method, in which the microgel charge is increased until the actual charge is achieved.

Simulations

In the simulation procedure the microgel particle is modeled as a network of cross-linked polymer chains. Monte Carlo simulations are carried out within a coarse-grained model for polyelectrolytes known as the bead–spring model. In this framework, monomer units of the polymer chain and ions are considered spheres, whereas the solvent is treated as a dielectric continuum. (24, 30) Each chain of the microgel consists of a sequence of 8 spherical monomer units (beads) connected by tetrafunctional cross-linkers of the same species than monomers. This number of monomers per chain can be considered typical for highly cross-linked networks. (35) The microgel simulated here is made of 206 chains connected by 133 cross-linkers. The charge of the microgel is conferred by adding beads of each chain with the negative elementary charge, e, as a result of having ionizable groups. In this work, we explore particles with 1 ionized group per chain. The simulation cell also contains ionic species, both cations and anions, as well as an excess of cations required to ensure an electroneutral system. The ions are also modeled as spheres, whose diameters are σ_{ion} = 0.7 nm including the corresponding hydration shell. This hydrated ion size is in agreement with the values experimentally estimated for some monovalent cations and anions by Israelachvili, (51) who compiled data from different techniques. However, for highly concentrated microgel suspensions, the effect of excluded volume interactions could be overestimated using this ion size, since the solvation shell of the ions becomes less relevant in those cases. For that reason, we have also performed simulations considering σ_{ion} = 0.4 nm, in order to discern whether steric repulsion still plays an important role. In addition, the former diameter used here could be representative for some drugs, such as theophylline or caffeine, (52) and may give an approximation of the excluded volume interactions in microgel–drug systems.

Interactions between all particles in the simulation cell are briefly summarized as follows (more details may be found in a previous work (53)). The short-range repulsion between any pair of particles (monomeric units or ions) due to excluded volume effects is modeled by means of the purely repulsive Weeks–Chandler–Andersen (WCA) potential: (27, 28, 54, 55)

$$V_{\mathrm{WCA}}(r) = \begin{cases} 4\epsilon_{\mathrm{WCA}}\left(\dfrac{\sigma^{12}}{r^{12}} - \dfrac{\sigma^{6}}{r^{6}} + \dfrac{1}{4}\right) & r \leq 2^{1/6}\sigma \\ 0 & r > 2^{1/6}\sigma \end{cases} \quad (12)$$

where r is the center to center distance between a given pair of particles, $\epsilon_{\mathrm{WCA}} = 4.11 \times 10^{-21}$ J, and $\sigma = (\sigma_i + \sigma_j)/2$, where σ_i is the particle diameter of component i. The interaction connecting monomer units and cross-linkers with their neighbors is modeled by harmonic bonds,

$$\beta V_{\mathrm{bond}}(r) = \frac{k_{\mathrm{bond}}}{2k_{\mathrm{B}}T}(r - r_0)^2 \quad (13)$$

where $k_{\mathrm{bond}} = 0.4$ N/m is the elastic constant and $r_0 = 0.65$ nm is the equilibrium bond length. All the charged species interact through the Coulomb potential

$$\beta V_{ij}^{\mathrm{elec}}(r) = \frac{z_i z_j l_{\mathrm{B}}}{r} \quad (14)$$

where z_i is the valence of species i.

The thermoresponsive character of microgels comes from hydrophobic forces. When nonpolar macromolecules are inserted into an aqueous medium, water molecules rearrange their hydrogen bonds and form a structure like a cage, generating a high degree of local order. When temperature increases, the total number of water molecules structured around the hydrophobic solute decreases. To minimize the loss of entropy, the number of nonpolar molecules exposed to the solvent is reduced aggregating them: the microgel shrinks. In this work, the hydrophobic force is modeled through an interaction potential that consists in a smooth approximation of the square-well potential (previously used by other authors (56, 57)) whose depth increases with temperature, given by the following equation:

$$V_{\mathrm{hyd}}(r) = -\frac{\varepsilon_{\mathrm{h}}(T)}{2}\{1 - \tanh[k_{\mathrm{h}}(r - r_{\mathrm{h}})]\} \quad (15)$$

where $\varepsilon_{\mathrm{h}}(T) < 0$ is the depth of the potential, r_{h} is its range, and k_{h} is fixed so that $V_{\mathrm{hyd}}(0.9\, r_{\mathrm{h}}) = 0.9\varepsilon_{\mathrm{h}}$. The potential depth obeys an increasing sigmoid function to reproduce the behavior of thermo-shrinking gels, (59)

$$\varepsilon_{\mathrm{h}}(T) = \frac{\varepsilon_{\max}}{2}\{1 + \tanh[k_{\varepsilon/2}(T - T_{\varepsilon/2})]\} \quad (16)$$

ε_{max} is the maximum depth of the hydrophobic potential and $k_{\varepsilon/2}$ is proportional to the slope of the function at the point where $\varepsilon_h(T_{\varepsilon/2}) = -\varepsilon_{max}/2$. The dependence of the interaction parameter ε_h with temperature is shown in the inset of Figure 2. The behavior of the potential is inspired in physical grounds from the model of hydrophobic interaction developed by Kolomeisky and Widom. (58) However, a previous work showed that this potential leads to unphysical volume fractions at high temperatures. (59) For that reason, a phenomenological potential with a limited depth has been preferred. The values of its parameters were obtained simultaneously matching several experimental data sets on six different microgels with different fraction of charged monomers and temperatures ranging from 10 to 60 °C. (35) In a subsequent work, (60) it was also checked that these parameters also justified the behavior of a poly(NIPAM)-based gel with a very different cross-linker density. It should be also mentioned that poly(NIPAM) is considered a model of thermoresponsive polymer, and other polymers with potential applications as drug carriers exhibit similar lower critical solution temperatures. (61, 62) Thus, realistic simulation results are expected (at least to some extent) if this potential is used. In any case, it should be kept in mind that this hydrophobic potential is operative only for uncharged monomers, since charged groups are considered hydrophilic rather than hydrophobic beads. Nevertheless, the choice of hydrophobic potential employed in the simulations and, in particular, the dependence of ε_h with T will depend on the specific nature of the polymer fibers of the microgel and the solvent conditions. Therefore, the results predicted in this work may experience some variations when applied to other kind of microgel particles. In spite of this, the predictions deduced in this work represent a good qualitative representation that illustrates the thermal response of real ionic solutions of microgels.

Simulations are performed using the canonical ensemble, in which volume, temperature and number of particles are kept constant. All the simulations are carried out in a cubic box with a length L and periodic boundary conditions. The simulation box is large enough to contain a single microgel particle and a significantly developed electric double layer around it. More specifically, L is calculated as $L \approx 2(R_0 + 4\, l_D)$, where R_0 is an estimate of the radius of the microgel in the absence of additional electrolyte and l_D is the Debye screening length. For instance, for 1 and 100 mM, the L-values employed are 100 and 34 nm, respectively, much larger than the Debye lengths (9.67 and 0.967 nm at 288 K, respectively). Thus, the microgel does not feel significantly the electrostatic repulsion of periodic images. The initial configuration of the microgel and their counterions used in the runs in the presence of salt were obtained from previous simulations in the absence of salt. After this preliminary equilibration, ions coming from the salt were added at random positions and the genuine run in the presence of salt started. Two types of MC moves were employed: (i) the usual single-particle displacements; (ii) rescaling of the positions of all the particles multiplying by a factor to reduce the thermalization time (see ref 33 for further details about this size rescaling). In this way, small changes in the size of the microgel (maximum 1%) were explored. In the single-particle moves, the maximum displacements of monomers and ions were individually adjusted to achieve acceptance ratios of 30–70%. In both equilibration runs, at least 10^8 MC moves were employed. To check that the equilibration had been reached, the evolution of some properties, such as the radius of gyration, was monitored averaging on batches of 5×10^4 steps. At least, 2×10^8 MC moves were employed for averaging. The electrostatic energy was computed through a classical implementation of Ewald sums, following some practical guidelines given by Linse. (63) The cutoff distance employed in the real space was $L/2$. The calculation of the reciprocal contribution to energy was estimated using sets of integers (n_x, n_y, n_z) that verified $(n_x^2 + n_y^2 + n_z^2)^2 \leq 4$ (reciprocal cutoff). The parameter characterizing the width of Gaussian charge distributions was $\alpha = 5/L$ (see review by Linse for notation and further details). The maximum relative error admitted in the real-space contribution to energy was 10^{-3}. Additional information about methods to compute long-range interactions can be found in the work by Arnold and Holm. (64)

Results and Discussion

Monte Carlo simulations were performed at two different concentrations of monovalent salt, 1 mM and 100 mM. We consider this salt to be NaCl, and assume ion sizes given by the corresponding effective hydrated diameters in conditions of high dilution. Their values are shown in Table 1, together with other properties of the microgel particle, namely the number of charged monomers in the microgel, the size of the composing monomers, and the temperature interval in which our study is performed.

Table 1. Input Parameters of Monte Carlo Simulations Used to Generate Microgel Particles in the Presence of Electrolyte

parameter	symbol	value
monomer diameter	σ_{mon}	0.65 nm
ion diameter	σ_{ion}	0.70 nm
microgel charge	Z	206 e
temperature	T	20–60 °C

Before comparing the simulation results with the theoretical predictions we show some results regarding the thermal response of the simulated microgel particles.

Thermal Response

Because of the fact that attractive hydrophobic interactions between monomers of the microgel are temperature dependent, the microgel becomes a thermoresponsive particle. This means that its internal morphology and the degree of swelling changes with temperature. The equilibrium conformation is a balance between many contributions, namely the hydrophobic, elastic and electrostatic forces. Therefore, the final equilibrium state not only depends on temperature but also on the electrolyte concentration. In order to determine the thermal response of the microgels we performed a total amount of 9 simulation runs with temperatures ranging from 20 to 60 °C for each salt concentration.

Figure 2 shows the microgel effective average radius R_m as a function of temperature. It is defined as $R_m = (5/3)^{1/2} R_g$, where R_g is the radius of gyration of the microgel particle. For a spherical microgel with a homogeneous distribution of mass, R_m represents the external radius of the microgel. As observed, the temperature range considered in this work provides different swelling ratios of the microgel particle. For low temperature, microgel particle is swollen, but when temperature is increased it undergoes a volume transition to shrunken states. The transition temperature is about 34 °C, which is consistent with the experimental response of many types of microgel particles.

Figure 2

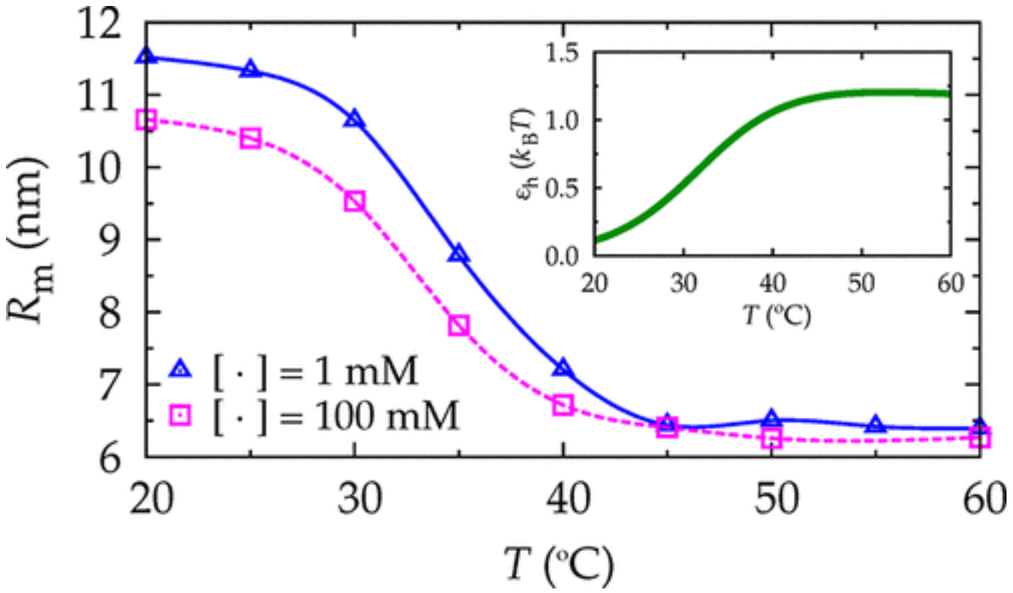

Figure 2. Average effective radius of the simulated microgel as a function of temperature for two salt concentrations, 1 mM and 100 mM. Error bars are not shown because they are smaller than the size of the symbols. In the inset, the depth of the potential ε_h used in the simulations is plotted against the temperature.

With regard to the response with the electrolyte concentration, the shrinking behavior as a function of temperature does not change significantly with the salt concentration. However, at the same temperature, for 100 mM the microgel radius is smaller than for 1 mM. This is a well-known reasonable result, caused by the screening of the microgel charge. In fact, for large electrolyte concentration, repulsive Coulombic interactions between monomers (which enhance the particle swelling) are more efficiently screened by the counterions. Consequently, the equilibrium swelling state shifts to more shrunken configurations. (1) In addition, the penetration of counterions exerts an osmotic pressure that induces the particle swelling. This pressure difference inside and outside the microgel is roughly inversely proportional to the salt concentration, (65) and this is why the swelling observed for 100 mM is less important than for 1 mM. Nevertheless, when microgel is collapsed at high temperature, the swelling state is dominated by monomer–monomer hydrophobic forces, so counterion effects become not very significant, leading to very similar values of R_m for both salt concentrations.

The volume change with the temperature is clearly appreciated in Figure 3, where the local concentration of polymers and charged monomers are plotted, as well as the snapshots of the microgel, at four different temperatures. As temperature increases, a progressive shrinking in the microgel structure becomes noticeable. In the swollen state, the internal morphology of the particle is consistent of large pores through which ions can penetrate, but as particle shrinks, the size of the pores decreases, even disappearing for high temperature. However, the decrease of the particle size with the temperature is not the only effect that arises. The internal structure is also affected, as shrunken microgels tend to arrange in a nonhomegeneous form in the inner region of the particle. This effect has been previously observed in small-sized microgels of few tens of nanometers similar to the ones employed in this work, where the typical length of the interconnected chains is of the same order of magnitude of the size of the particle. As mentioned above, charged monomers are considered hydrophilic (rather than hydrophobic) beads, thus they are not attracted by the uncharged ones. What is more, when uncharged beads collapse due to attractive hydrophobic forces, they would tend to segregate the hydrophilic monomers to minimize the free energy. Consequently, many of the charged beads would be displaced toward the outer and inner surfaces of the monomer clusters, as shown in the figure for high temperature. In some cases, a few interconnected voids can also be formed in this segregation process instead of a unique hollow. (33)

Figure 3

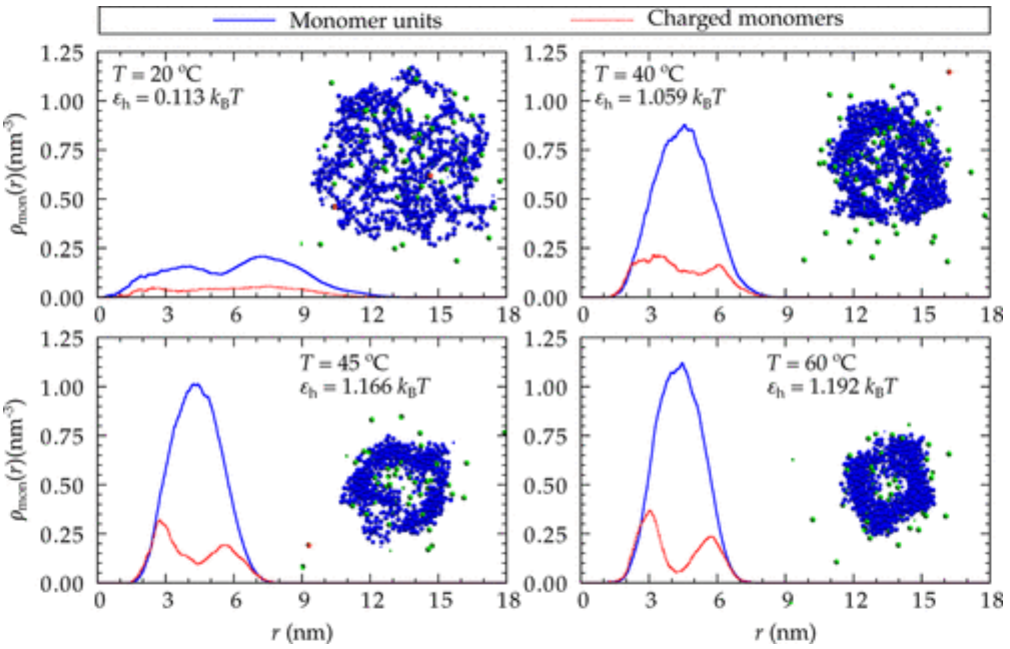

Figure 3. Polymer (formed by neutral monomers, charged monomers, and cross-linkers) and charged monomer concentration as a function of the distance to microgel center, for different temperatures and hence distinct deph of hydrophobic potential and degree of swelling. For each temperature, a slice of the central part of the simulation box is shown, where cross sections of the microgel particles can be visualized. Swollen microgels show a more homogeneous structure than the shrunken ones, in which an inner hole is formed. Green spheres represent counterions, while orange ones represent coions.

Simulation results not only provide the mass and charge distribution of the microgel network, but also the density profiles of counterions and coions inside and around the particle. In the following sections we discuss these properties. We first analyze the results in terms of a global property such as the effective microgel charge, and then we discuss in more detail the local properties by studying the radial distribution function of counterions. Simulation data are compared to the theoretical predictions applying the two models for the steric interaction described in eq 8. For this purpose, we make use of the local polymer volume fraction, $\phi(r)$, and the local distribution of charged monomers, $\rho_c(r)$ as input parameters to determine the microgel-ion electrostatic and steric interactions (see eqs 4, 5, and 8). Then, these interactions are employed in the Ornstein–Zernike integral equation method to finally obtain the ionic radial distribution functions, $g_{m+}(r)$ and $g_{m-}(r)$. They can be compared to the simulated ones to check whether the theory is able to properly account for the effect of the steric interaction in conditions of charge and mass heterogeneity.

Effective Charge

A very useful way to quantify the global efficiency of the ionic permeation inside a microgel is to study the effective charge of the microgel particle, Z_{eff}. It is straightforwardly calculated from ionic density profiles inside the microgel particle as

$$Z_{\mathrm{eff}} = -Z + 4\pi \int_0^{R_m} [\rho_{m+}(r) - \rho_{m-}(r)] r^2 \, \mathrm{d}r \quad (17)$$

where Z is the number of charged monomers of the microgel. The ionic density profiles $\rho_{m+}(r)$ and $\rho_{m-}(r)$ have been calculated from their radial distribution functions through eq 11.

The effective charge is very helpful to characterize the permeation as a function of the swelling ratio because it is very sensitive to swelling and shrinking of microgel particle. For this reason, it has been previously employed to study the steric interaction. (36) If counterions penetrate inside the microgel, Z_{eff} is expected to decrease owing to screening of the bare charge. On the contrary, if counterions cannot permeate, they accumulate in a external shell around the microgel, leading to a weaker charge screening, and so to a higher value of the effective charge.

In principle, one would expect an increase of the effective charge with temperature. First, because an increase of the temperature leads to a weakening of the electrostatic attraction of counterions to the microgel particle (compared to the thermal energy, $k_B T$), so counterions are less likely to diffuse inside, enhancing the effective charge. Second, because the reduction of the microgel size with temperature implies that it is necessary to concentrate the internal counterions in a much smaller volume. Hence, the electrostatic repulsion between pairs of counterions pushes some of them out of the particle, leading to an increase of Z_{eff} too. Finally, the particle shrinking at high temperatures causes an increase of the polymer volume fraction, which enhances the steric repulsion between counterions and the polymer network. As a consequence of this, counterions are expelled from the interior of the particle in shrunken configurations, which makes charge screening lower than if they did not interact sterically.

Figure 4 displays the average values of Z_{eff} obtained in the simulations as a function of temperature (symbols) for the two studied electrolyte concentrations, assuming $\sigma_i = 0.7$ nm for the ion diameter (numerical errors below 5% in all cases). The monotonic increase of the effective charge with temperature may be clearly observed for a salt concentration of 100 mM (see top graph of Figure 4). However, for 1 mM (bottom graph) this increase is weaker and some fluctuations arise. This effect can be attributed to the existence of inhomogeneities in the distribution of the microgel bare charge. As shown above, the charge and mass distribution of the small-sized microgel develop an internal region with low polymer concentration surrounded by a corona of high density. This heterogeneous morphology provides plenty of space in the center of the particle, so counterions are able to better accommodate inside, avoiding counterion-counterion repulsion. The charge heterogeneity induces a decrease of $|Z_{\mathrm{eff}}|$ and competes with the effect of the counterion obstruction explained above. The reason why this effect becomes less important at high salt concentration relies simply on the screening of the electrostatic forces.

Figure 4

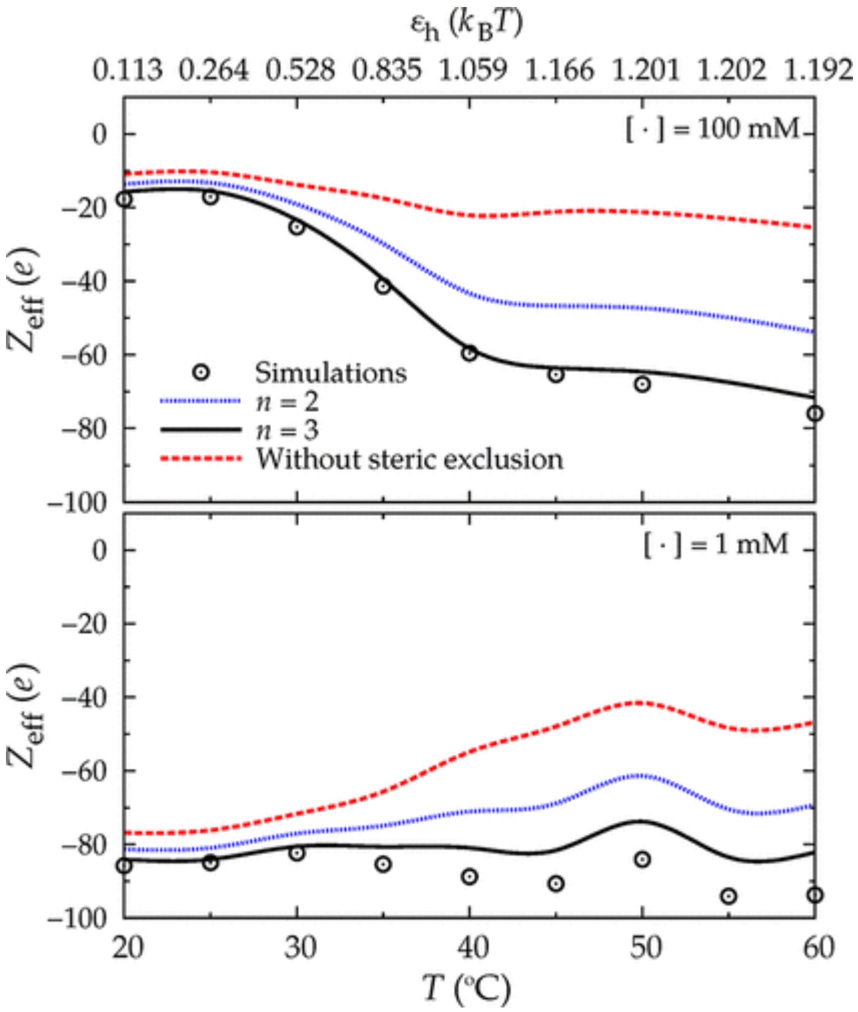

Figure 4. Microgel effective charge as a function of temperature. Black dots stand for Z_{eff} measured in simulations, while the curves are theoretical predictions calculated by solving Ornstein–Zernike (OZ) equations for three different cases: taking into account $n = 2$ and $n = 3$ in eq 8 for steric interaction, and ignoring the steric repulsion, $V_{mister}(r) = 0$. The top graph has been obtained considering 100 mM of electrolyte concentration, while the bottom one corresponds to 1 mM. Error bars are not shown because they are smaller than the size of the symbols. The top x axis shows the deph of the hydrophobic potential for each temperature considered, but note that the values are not scaled.

Figure 4 also shows the theoretical results obtained under three different approximations. In the first one we neglect the steric repulsion and assume that microgel and ions interact exclusively through electrostatic interactions (dashed line). In the other two situations the steric effect is included using two different exponents in eq 8: $n = 2$ and $n = 3$ (dotted and solid lines, respectively).

One of the most remarkable results that we may extract from the comparison between simulations and theory is that the microgel-ion steric repulsion should be considered in the model to account for the counterion permeation in shrunken microgels, at least for ionic sizes comparable to or larger than $\sigma_i = 0.7$ nm, the ones studied here. As can be seen, the curve obtained by solving Ornstein–Zernike equations neglecting volume exclusion effects overestimates the charge screening effect for both salt concentrations at high temperatures (high polymer volume fractions). In other words, in the absence of steric repulsion, the electrostatic interaction alone can sometimes lead to values of Z_{eff} smaller than the ones observed in simulations. However, this Figure also shows that the effect of the steric repulsion is not so important for swollen microgels (low temperatures in our case). In fact, Claudio et al. (31) succeeded in reproducing the ionic distribution of a microgel in a good solvent using a Poisson–Boltzmann model (that does not account for excluded volume effects).

When including the steric effect, we see that the results obtained using $n = 3$ in eq 8 provides much better quantitative agreement with simulations than those obtained with the Ogston model ($n = 2$). In fact, the Ogston model underestimates the steric repulsion leading to a smaller values of $|Z_{\mathrm{eff}}|$ compared to simulation data. This means that an assembly of randomly placed spheres provides a more accurate representation of the internal morphology of the microgel than a network of long rigid fibers. This is a quite reasonable conclusion, given that polymer fibers are treated in our simulations as being formed by short interconnected chains with only 8 spherical monomers. However, it should be pointed out that these results do not imply that the use of $n = 3$ in eq 8 is always more accurate than the Ogston model for any polymer network in equilibrium with a permeating solute. For instance, previous simulation studies of macroscopic gels show that the permeation of large solutes inside cross-linked polymer networks with very long polymer fibers is better described by the Ogston model. (45) This is because, under such conditions, the chain-like geometry dominates, playing the monomer shape a minor role.

As observed from Figure 4 the agreement between theoretical predictions with $n = 3$ and simulations is excellent for 100 mM. For 1 mM the model still yields quite good quantitative agreement in the swollen configuration, but overestimates the counterion permeation about a 10% in the shrunken state. This deviation comes from the very strong density variations of the ionic density profiles arising inside the microgel. Indeed, as will be shown below, at high temperatures and low electrolyte concentration, the internal heterogeneities cause changes of the density of counterions by a factor larger than 100 that the OZ-HNC integral equation theory is not able to completely reproduce.

Figure 5

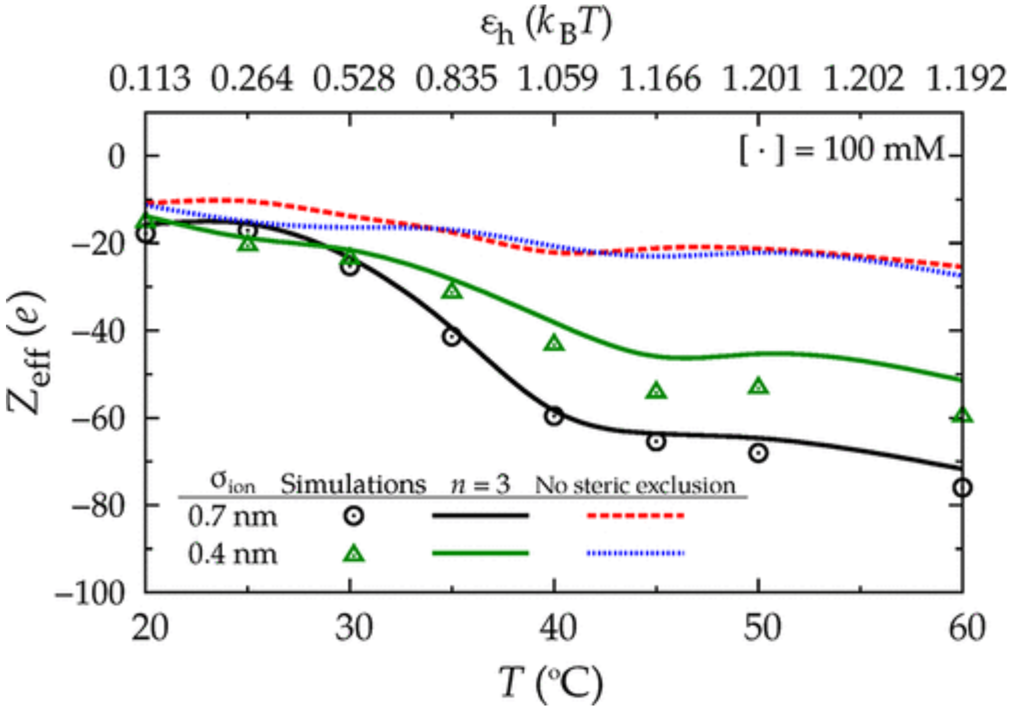

Figure 5. Microgel effective charge as a function of temperature for 100 mM of electrolyte concentration and two different sizes of ions. Black color is used for σ_i = 0.7 nm, while green color represents σ_i = 0.4 nm. Symbols stand for Z_{eff} measured in simulations, while solid lines are theoretical predictions calculated by solving OZ equations, using n = 3 in eq 8 for steric interaction. Red dashed line and blue dotted line are calculated ignoring the steric repulsion for σ_i = 0.7 nm and σ_i = 0.4 nm, respectively.

To confirm whether steric interaction may affect the microgel effective net charge even when there is no hydration shell around the ions, another set of Monte Carlo simulations and Ornstein–Zernike calculations were performed at high concentration (100 mM) using a smaller value for the ion diameter, namely σ_i = 0.4 nm. These results are compared in Figure 5 with those obtained for σ_i = 0.7 nm. It is clearly shown that both simulations and theoretical results follow the same trend for σ_i = 0.4 nm and σ_i = 0.7 nm, although the effective charge absolute values in shrunken states are smaller for smaller ions. This is an expected result, since a decrease of the ion size diminishes the steric repulsion between the microgel and the counterions, which leads to larger counterion permeation for σ_i = 0.4 nm, and hence to an increase of microgel charge screening. However, in swollen states there is no significant difference due to ion diameter, since excluded volume interactions become less relevant for expanded microgels, as mentioned above. In addition, as in Figure 4, the curve obtained by solving Ornstein–Zernike equations neglecting volume exclusion effects strongly overestimates the charge screening effect for both ion sizes at high packing fractions.

Ionic Density Profiles

Here, we complete the data of effective charge with additional detailed information about the local density profiles of the ions inside and around the microgel particle. Figures 6 and 7 show the radial distribution functions of counterions for different temperatures and hence different swollen states. The plots include the simulation results (dashed blue line), and the theoretical predictions with and without considering excluded volume interactions (green and pink solid lines, respectively). Coion density profiles are not shown since they do not contribute with significant insights in the physical interpretation. First, we discuss the simulation results. As it could be observed in both Figures, at low temperature (swollen state), counterions can easily diffuse through microgel pores, so they are homogeneously distributed in the internal region. However, as temperature increases and microgel shrinks, two maxima begin to rise in $g_{m+}(r)$. As mentioned above, the morphology of such small microgel particle becomes heterogeneous for shrunken states, in which charged monomers become reallocated so that they tend to form an inner charged spherical shell and an external one. As a consequence of this, counterions tend to congregate close to both shells, inside the particle (first maximum) or around the microgel (second maximum). A schematic explanation of this phenomenon is drawn in Figure 8.

Figure 6

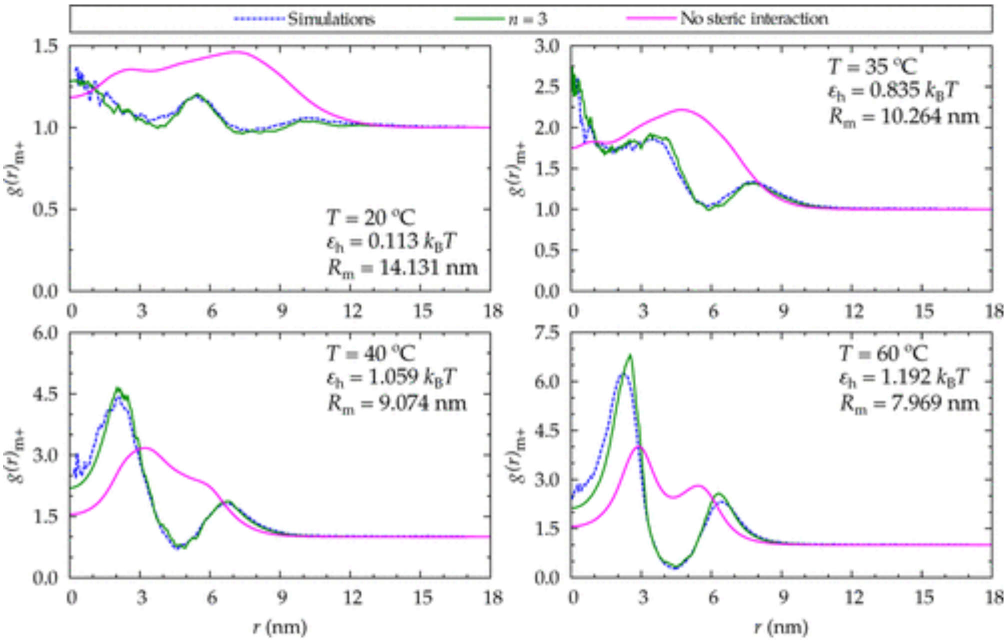

Figure 6. Radial distribution functions of counterions as a function of the distance to microgel center, for different temperatures and hence distinct deph of hydrophobic potential and degree of swelling. All curves correspond to a salt concentration 100 mM. Dashed blue line has been obtained directly from simulations, while solid lines represent $g_{m+}(r)$ calculated by solving Ornstein–Zernike integral equations: taking

into account steric repulsion from eq 8 with n = 3 (green) and considering that there is no steric interaction (pink).

Figure 7

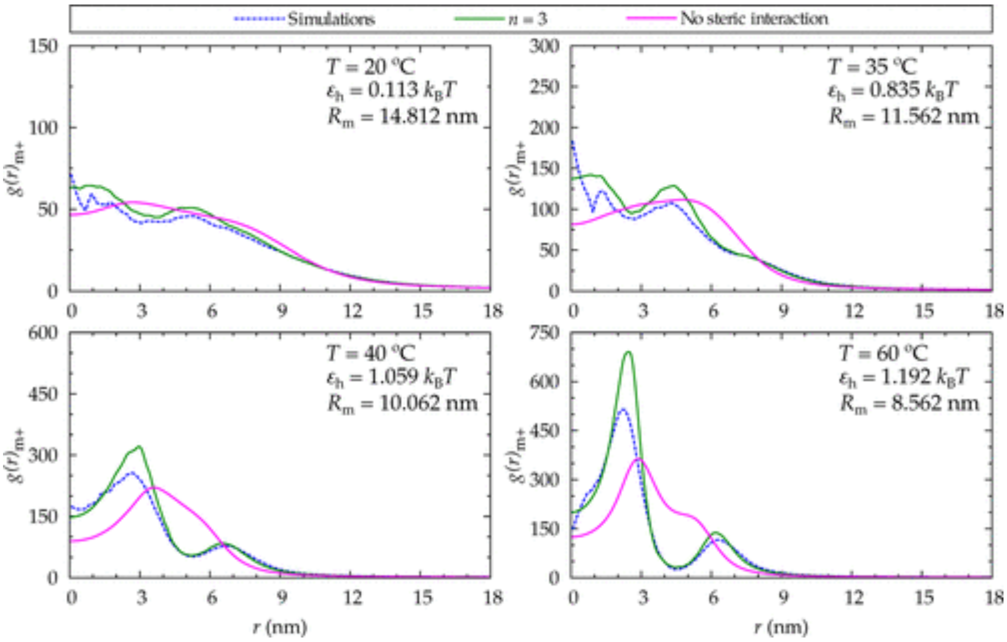

Figure 7. Radial distribution functions of counterions as a function of the distance to microgel center, for different temperatures and hence distinct deph of hydrophobic potential and degree of swelling. All curves correspond to a salt concentration 1 mM. Dashed blue line has been obtained directly from simulations, while solid lines represent $g_{m+}(r)$ calculated by solving Ornstein–Zernike integral equations: taking into account steric repulsion from eq 8 with n = 3 (green) and considering that there is no steric interaction (pink).

Figure 8

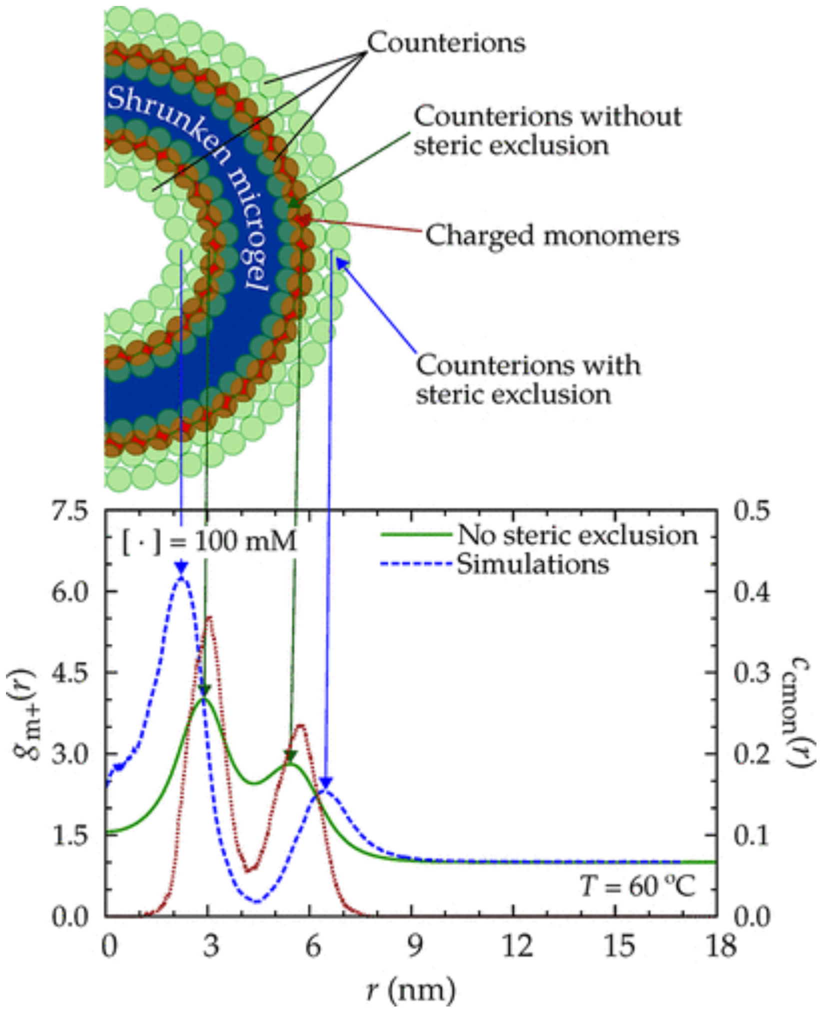

Figure 8. Explanation of the two maxima observed in radial distribution function of counterions inside and around the shrunken microgel particle. Dashed blue line represents simulation results, while green solid line stands for theoretical results ignoring steric exclusion. In the picture, green circles represent counterions and red circles are the charged monomers allocated in both shells.

Theoretical predictions are also able to reproduce the appearance of these two maxima in the counterion concentration as microgel collapses. In fact, both peaks are observed even in the limit of vanishing steric interactions (see pink solid line), which indicates that this phenomenon is mainly induced by the electrostatic attraction between counterions and the heterogeneous distribution of bare charges inside the microgel. There is, however, a subtle distinction: these maxima are situated closer to the charged shells because counterions are not affected by volume exclusion. As soon as the steric contribution is taken into account (using eq 8 with $n = 3$), the internal maximum shifts to smaller r, whereas the external one moves to larger values of r, due to the counterion exclusion exerted by the polymer fibers in the spherical shell.

The comparison between theory and simulations clearly points out that neglecting the microgel–ion steric interaction may lead to acceptable predictions for the counterion density profiles at 1 mM if microgels are swollen enough, but wrong predictions for shrunken states or high electrolyte concentration. However, when the steric interaction is included in the model, qualitative and even quantitative agreement are achieved for the whole set of swelling states. The agreement is specially good for swollen states, and worsens in the shrunken states for 1 mM, where the model overestimates the concentration of counterions in the internal layer. We attribute these discrepancies to the accuracy of the HNC approximation. This closure works in general very well for the kind of potentials used in this work, but it should be reminded that HNC ignores the so-called bridge function in the potential of mean force, which takes into account strong correlations at short distances. (66) In particular, previous calculations performed in charged colloidal suspensions show that the colloid-ion bridge function contributes with an additional attraction. (67, 68) Therefore, it is also expected that our theory predicts an overestimation of the counterion adsorption at low electrolyte concentration in the shrunken states, since in this case the density charge of the microgel is larger and weakly screened by the counterion cloud. In spite of this, HNC still provide a qualitative agreement in this situation, and has the additional advantage of being very simple to numerically implement, in contrast with other more sophisticated closure relations.

Therefore, we can confirm that the steric microgel–ion interaction plays an important role on the ionic distribution inside the microgel particle, specially close to the collapsed state. Moreover, the model proposed in eq 8 has shown to be accurate enough to correctly described the simulated ionic density profiles, even in the case of nonhomogeneous distribution of internal mass and charge of the microgel particle.

Conclusions

In this work, we study the effect of the steric excluded-volume repulsion exerted by the fibrous polymer network of the microgel on the ionic permeation, for different swelling states and concentrations of monovalent salt. In particular, we focus on the effective charge of the microgel and the local ionic density profiles around and inside the microgel. For this purpose, Monte Carlo simulations are compared to the theoretical predictions assuming that the suspension is a ternary mixture of microgels, counterions and coions, and solving the corresponding OZ integral equations within the HNC approximation.

The results show that splitting the microgel–ion interaction into electrostatic and steric terms is a good approximation. Moreover, the comparison with simulation data also indicates that the internal structure of the microgel cross-linked fibrous structure is better represented by a collection of randomly placed spherical monomers. An advantage of this model is that the effective steric microgel–ion repulsive interaction can be calculated analytically. This approach for the internal morphology of the microgel works well for the kind of system we are dealing, namely, small highly cross-linked microgel with few monomers per chain permeated by ions with size of the order of the monomer unit. However, it should be emphasized that, for larger microgels, particles with longer polymer chains between cross-linker nodes may be better represented by a random assembly of cylinders rather than spheres. (45)

In conclusion, our work reveals that the steric interaction should be included to correctly account for the ion distributions if the polymer volume fraction of the microgel and ionic sizes are large enough. Under such circumstances, ignoring this contribution could lead to an artificial enhancement of the counterion permeation and, so, to a significant decrease of the microgel effective charge. Once this effect is included, the theoretical model is able to correctly describe the response of the effective charge to swelling and shrinking of the microgel particle, and provides a quantitative account for the ionic density profiles, even in situations of heterogeneous charge and mass distributions inside the particle. Moreover, our predictions could be also interesting to understand the ionic permeation inside nonhomogeneous hollow thermoresponsive microgels, like the ones studied by Dubbert et al. (69)

Future investigations will focus on the effect of ion specificity on the swelling behavior of the microgel. As shown in previous work, (37) hydrophobic ions tend to accumulate in specific locations of the polymer network, leading to new effects that go far beyond charge screening, such as charge inversion and overcharging phenomena. Therefore, it would be interesting to compare simulation and theoretical data also in this situation, given the importance of microgels as carriers of hydrophobic solutes and biomolecules. (9, 70)

Author Information

Corresponding Author

Arturo Moncho-Jordá - *Departamento de Física Aplicada, Facultad de Ciencias, Universidad de Granada, Campus Fuentenueva S/N, 18071 Granada, Spain*; Email: moncho@ugr.es

Authors

Irene Adroher-Benítez - *Departamento de Física Aplicada, Facultad de Ciencias, Universidad de Granada, Campus Fuentenueva S/N, 18071 Granada, Spain*
Silvia Ahualli - *Departamento de Física, Escuela Politécnica Superior de Linares, Universidad de Jaén, 23700 Linares, Jaén, Spain*
Alberto Martín-Molina - *Departamento de Física Aplicada, Facultad de Ciencias, Universidad de Granada, Campus Fuentenueva S/N, 18071 Granada, Spain*

Manuel Quesada-Pérez - *Departamento de Física, Escuela Politécnica Superior de Linares, Universidad de Jaén, 23700 Linares, Jaén, Spain*

Acknowledgment

The authors thank the Spanish “Ministerio de Econimı́a y Competitividad (MINECO), Plan Nacional de Investigación, Desarrollo e Innovación Tecnológica (I+D+i)” (Projects MAT2012-36270-C02 and -04), the European Regional Development Fund (ERDF), and “Consejerı́a de Innovación, Ciencia y Empresa de la Junta de Andalucı́a” (Project P09-FQM-4698) for financial support.

References

1. Sierra-Martín, B.; Lietor-Santos, J. J.; Fernández-Barbero, A.; Nguyen, T. T.; Fernández-Nieves, A. In Microgel Suspensions: Fundamentals and Applications; Fernández-Nieves, A.; Wyss, H.; Mattsson, J.; Weitz, D., Eds.; 2011; Wiley-VCH: Weinheim, Germany, p 461.

2. Murray, M. J.; Snowden, M. J. Adv. Colloid Interface Sci. **1995**, 54, 73– 91

3. Saunders, B. R.; Vincent, B. Adv. Colloid Interface Sci. **1999**, 80, 1– 25

4. Saunders, B. R.; Laajam, N.; Daly, E.; Teow, S.; Hu, X.; Stepto, R. Adv. Colloid Interface Sci. **2009**, 147–148, 251– 262

5. Lee, S. M.; Nguyen, S. T. Macromolecules **2013**, 46, 9169– 9180

6. Lee, S. M.; Bae, Y. C. Macromolecules **2014**, 47, 8394– 8403

7. Du, A. W.; Stenzel, M. H. Biomacromolecules **2014**, 15, 1097– 1114

8. Vinogradov, S. V. Nanomedicine **2010**, 5, 165– 168

9. Hoare, T.; Pelton, R. Langmuir **2008**, 24, 1005– 1012

10. Malmsten, M.; Bysell, H.; Hansson, P. Curr. Opin. Colloid Interface Sci. **2010**, 15, 435– 444

11. Ramos, J.; Peláez-Fernández, M.; Forcada, J.; Moncho-Jordá, A. In Soft Nanoparticles for Biomedical Applications; Callejas-Fernández, J.; Estelrich, J.; Quesada-Pérez, M.; Forcada, J., Eds.; The Royal Society of Chemistry: Cambridge, U.K., 2014; pp 133– 156.

12. Shin, J.; Cherstvy, A. G.; Metzler, R. Phys. Rev. X **2014**, 4, 21002

13. Moncho-Jordá, A.; Anta, J. A.; Callejas-Fernández, J. J. Chem. Phys. **2013**, 138, 134902– 13

14. Denton, A. R. Phys. Rev. E **2003**, 67, 011804– 011810

15. Gottwald, D.; Likos, C. N.; Kahl, G.; Löwen, H. Phys. Rev. Lett. **2004**, 92, 068301– 4

16. Colla, T.; Likos, C. N.; Levin, Y. J. Chem. Phys. **2014**, 141, 234902– 11

17. Johnson, E. M.; Deen, W. M. J. Colloid Interface Sci. **1996**, 178, 749– 756

18. Quesada-Pérez, M.; Adroher-Benítez, I.; Maroto-Centeno, J. A. J. Chem. Phys. **2014**, 140, 204910– 7

19. Ulrich, S.; Laguecir, A.; Stoll, S. Macromolecules **2005**, 38, 8939– 49

20. Reddy, G.; Yethiraj, A. Macromolecules **2006**, 39, 8536– 42

21. Chang, R.; Yethiraj, A. Macromolecules **2006**, 39, 821– 828

22. Jiang, T.; Wu, J. J. Phys. Chem. B **2008**, 112, 7713– 7720

23. Dias, R. S.; Pais, A. Adv. Colloid Interface Sci. **2010**, 158, 48– 62

24. Stoll, S. In Soft Nanoparticles for Biomedical Applications; Callejas-Fernández, J.; Estelrich, J.; Quesada-Pérez, M.; Forcada, J., Eds.; The Royal Society of Chemistry: Cambridge, U.K., 2014, pp 342– 371.

25. Cherstvy, A. G. J. Phys. Chem. B **2010**, 114, 5241– 5249

26. Ghosh, S. K.; Cherstvy, A. G.; Metzler, R. J. Chem. Phys. **2014**, 141, 074903

27. Mann, B. A.; Holm, C.; Kremer, K. J. Chem. Phys. **2005**, 122, 154903– 14

28. Yin, D.-W.; Olvera de la Cruz, M.; de Pablo, J. J. J. Chem. Phys. **2009**, 131, 194907

29. Yan, Q.; de Pablo, J. J. Phys. Rev. Lett. **2003**, 91, 018301

30. Košovan, P.; Richter, T.; Holm, C. Prog. Colloid Polym. Sci. **2013**, 140, 205– 221

31. Claudio, G. C.; Kremer, K.; Holm, C. J. Chem. Phys. **2009**, 131, 094903– 9

32. Jha, P. K.; Zwanikken, J. W.; Detcheverry, F. A.; de Pablo, J. J.; Olvera de la Cruz, M. Soft Matter **2011**, 7, 5965– 5975

33. Quesada-Pérez, M.; Martín-Molina, A. Soft Matter **2013**, 9, 7086– 7094

34. Kobayashi, H.; Winkler, R. Polymers **2014**, 6, 1602– 1617

35. Quesada-Pérez, M.; Ramos, J.; Forcada, J.; Martín-Molina, A. J. Chem. Phys. **2012**, 136, 244903– 9

36. Moncho-Jordá, A. J. Chem. Phys. **2013**, 139, 064906– 12

37. Moncho-Jordá, A.; Adroher-Benítez, I. Soft Matter **2014**, 10, 5810– 5823

38. Guerrero-García, G. I.; González-Tovar, E.; Lozada-Cassou, M.; de J Guevara-Rodríguez, F. J. Chem. Phys. **2005**, 123, 34703– 20

39. Fernández-Nieves, A.; Fernández-Barbero, A.; Vincent, B.; de las Nieves, F. J. Macromolecules **2000**, 33, 2114– 2118

40. Belloni, L. J. Phys.: Condens. Matter **2000**, 12, R549– R587

41. Sing, C.; Zwanikken, J.; Olivera de la Cruz, M. Macromolecules **2013**, 46, 5053– 5065

42. Polotsky, A. A.; Plamper, F. A.; Borisov, O. V. Macromolecules **2013**, 46, 8702– 8709

43. Arndt, M. C.; Sadowski, G. J. Phys. Chem. B **2014**, 118, 10534– 10542

44. CRC Handbook of Chemistry and Physics, 69th ed., Weast, R. C., Ed.; CRC Press Inc.: Boca Raton, FL, 1988; p 2400.

45. Ahualli, S.; Martín-Molina, A.; Quesada-Pérez, M. Phys. Chem. Chem. Phys. **2014**, 16, 25483– 25491

46. Lazzara, M. J.; Blankschtein, D.; Deen, W. M. J. Colloid Interface Sci. **2000**, 226, 112– 122

47. Ogston, A. G. Trans. Faraday Soc. **1958**, 54, 1754– 1757

48. Bosma, J. C.; Wesselingh, J. A. J. Chromatogr. B. Biomed. Sci. Appl. **2000**, 743, 169– 180

49. Hansen, J. P.; McDonald, I. R. Theory of simple liquids, 3rd ed.;Academic Press: Amsterdam, 2006; Vol. 104, p 416.

50. Shah, N. H. Numerical Methods with C++ Programming; PHI Learning Pvt. Ltd.: New Delhi, 2009; p 325.

51. Israelachvili, J. N. Intermolecular and Surface Forces, 3rd. ed.; Academic Press: San Diego, CA, 2011; p 674.

52. Dursch, T. J.; Taylor, N. O.; Liu, D. E.; Wu, R. Y.; Prausnitz, J. M.; Radke, C. J. Biomaterials **2014**, 35, 620– 629

53. Quesada-Pérez, M.; Ahualli, S.; Martín-Molina, A. J. Chem. Phys. **2014**, 141, 124903– 11

54. Mann, B. A.; Everaers, R.; Holm, C.; Kremer, K. Europhys. Lett. **2004**, 67, 786– 792

55. Yin, D.-W.; Yan, Q.; de Pablo, J. J. J. Chem. Phys. **2005**, 123, 174909

56. Escobedo, F. A.; de Pablo, J. J. J. Chem. Phys. **1996**, 104, 4788– 4801

57. Khan, M. O.; Mel'nikov, S. M.; Jönsson, B. Macromolecules **1999**, 32, 8836– 8840

58. Kolomeisky, A. B.; Widom, B. Faraday Discuss. **1999**, 112, 81– 89

59. Quesada-Pérez, M.; Ibarra-Armenta, J. G.; Martín-Molina, A. J. Chem. Phys. **2011**, 135, 094109– 10

60. Quesada-Pérez, M.; Maroto-Centeno, J. A.; Martín-Molina, A. Macromolecules **2012**, 45, 8872– 8879

61. Pelton, R. Adv. Colloid Interface Sci. **2000**, 85, 1– 33

62. Ramos, J.; Imaz, A.; Callejas-Fernández, J.; Barbosa-Barros, L.; Esterrich, J.; Quesada-Pérez, M.; Forcada, J. Soft Matter **2011**, 7, 5067– 5082

63. Linse, P. Adv. Polym. Sci. **2005**, 185, 111– 162

64. Arnold, A.; Holm, C. Adv. Polym. Sci. **2005**, 185, 59– 109

65. Barrat, J.-L.; Joanny, J.-F.; Pincus, P. J. Phys. II **1992**, 2, 1531– 1544

66. Iyetomi, H.; Ogata, S.; Ichimaru, S. Phys. Rev. A **1992**, 46, 1051– 1058

67. Anta, J. A.; Bresme, F.; Lago, S. J. Phys.: Condens. Matter **2003**, 15, S3491– S3507

68. Quesada-Pérez, M.; Martín-Molina, A.; Hidalgo-Álvarez, R. J. Chem. Phys. **2004**, 121, 8618–8626

69. Dubbert, J.; Honold, T.; Pedersen, J. S.; Radulescu, A.; Drechsler, M.; Karg, M.; Richtering, W. Macromolecules **2014**, 47, 8700– 8708

70. López-León, T.; Elaïssari, A.; Ortega-Vinuesa, J. L.; Bastos-González, D. ChemPhysChem **2007**, 8, 148– 156